Springs, Rings, and Spirals of Rutile-Structured Tin Oxide Nanobelts
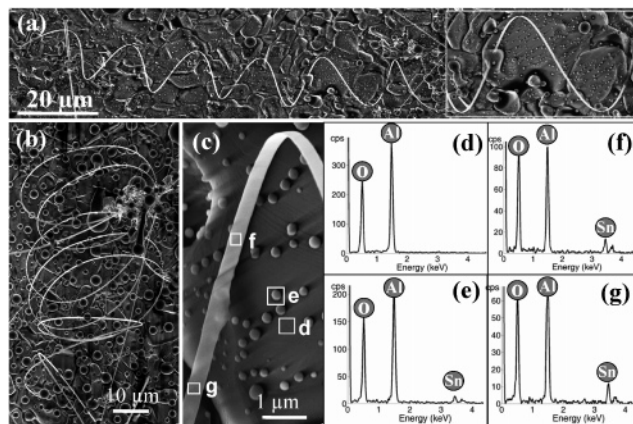
Rusen Yang[†] and Zhong Lin Wang*,[†,‡]

School of Materials Science and Engineering, Georgia Institute of Technology, Atlanta, Georgia 30332-0245, and National Center of Nanoscience and Technology, and College of Engineering, Peking University, Beijing, China

Received November 16, 2005; E-mail: zhong.wang@mse.gatech.edu

Synthesis of nanomaterials with well-controlled size, morphology, and chemical composition may open new opportunities in exploring a material's chemical and physical properties. Since the discovery of semiconducting oxide nanobelts[1] (ZnO, SnO_2, CdO, Ga_2O_3, and PbO_2) in 2001, nanobelts have been found and widely investigated in numerous materials including but not limited to[2] (Zn, Si, and C) II−IV semiconductors[3] (ZnS, CdSe, and ZnSe) and some other compounds[1,4] (In_2O_3, Ge_3N_4, Bi_2S_3, SiC, GaP, and $Pb_3O_2Cl_2$). Among these materials, wurtzite-structured ZnO is the most outstanding member. The uniqueness of the wurtzite structure is its noncentral symmetry and the surface polar charges due to the cation- and anion-terminated surfaces, such as Zn^{2+}-terminated (0001) and O^{2-}-terminated (000$\bar{1}$). To minimize the electrostatic interaction energy among the polar charges, the nanobelt dominated by the ±(0001) polar surfaces tends to fold over, resulting in the formation of single-crystalline nanorings, nanosprings, and nanospirals.[5] The reduction in the area of polar surfaces causes a structural transformation of a single-crystal ZnO nanobelt into a superlattice-structured, partial-polar surface dominated nanobelt, which eventually forms a rigid nanohelix.[6] Besides the nanorings observed for wurtzite AlN due to polar surfaces,[7] no report has been found on the formation of single-crystalline rings/springs/spirals for a material that has a structure different from wurtzite.

In this paper, we report for the first time the discovery of single-crystalline SnO_2 springs, rings, and spirals, which have the rutile structure. The grown nanostructures are made of tetragonal SnO_2 with the (011) polar surfaces facing toward the center. The formation process has been analyzed based on the polar charge interaction model. The discovery of SnO_2 rings and springs presents another family of polar surface dominated growth phenomena in a nonwurtzite-structured material, indicating the possibility of forming similar structures for other materials, such as TiO_2. Considering the important application of SnO_2 in sensors, these structures are not only ideal systems for fundamental understanding of the polarization effect on the morphology at the nanoscale level, but they also have potential applications[8] as nanoscale sensors, resonators, and transducers.

SnO_2 nanostructures were synthesized through a solid−vapor process in a horizontal tube furnace. The experimental apparatus has been described elsewhere.[9] After the tube had been evacuated to a pressure of 1×10^{-3} Torr, commercial SnO powders (Alfa Aesar) in the middle of the tube were heated to 800 °C, held for 90 min, heated again up to 1100 °C and held for another 50 min to complete the synthesis of the SnO_2 nanostructures. The Ar carrier gas was flowed through the system at a rate of 50 sccm (standard cubic centimeters per minute) under a constant pressure of 300 mbar during the entire synthesis process. The grown nanostructures were collected using a polycrystalline Al_2O_3 substrate placed downstream in the tube furnace at a temperature range of 600−700 °C.

[†] Georgia Institute of Technology.
[‡] National Center of Nanoscience and Technology and Peking University.

Figure 1. Scanning electron microscopy (SEM) and energy-dispersive X-ray spectroscopy (EDS) of SnO_2 nanostructures. (a) SEM image of a ZnO nanospring. (Inset) An enlarged image of the nanospring. (b) SEM image of SnO_2 nanospirals. (c) A higher magnification SEM image from the nanospring indicated in (a). (d−g) EDS spectra acquired from the areas labeled with d, e, f, and g in panel c, respectively.

We first examined the as-synthesized product by scanning electron microscope (SEM) in conjunction with energy-dispersive X-ray spectroscopy (EDS). We found that SnO_2 nanobelts tend to bend while they grow longitudinally. As a result, numerous SnO_2 spirals formed on the substrate. In addition, springs and rings were also found in the grown product. Figure 1a shows a SnO_2 spring lying on an Al_2O_3 substrate. The helical structure is made of a uniformly curved SnO_2 nanobelt with a pitch distance of ∼20 μm. The most common SnO_2 spirals are shown in Figure 1b, in which the curvature of the SnO_2 nanobelt changed during its growth. Most spirals/rings have diameters of 10−50 μm. A magnified part of the spring from Figure 1a is given in Figure 1c, showing clearly a belt-like geometry with a width of ∼300 nm and a thickness of several tens of nanometers. In addition, numerous nanoparticles are also formed on the Al_2O_3 substrate. To investigate the chemical composition of the product, we took EDS spectra from a series of locations along the nanobelt, on the nanoparticles, and on the blank substrate, as labeled from d−g in Figure 1c, and the results are displayed in Figure 1d−g, respectively. The EDS spectrum in Figure 1d shows only Al and O peaks with an atomic ratio close to 2:3, which is consistent with the composition of the underneath Al_2O_3 substrate. The absence of a Sn peak or any other peaks excludes a possible layer of SnO_2 or Sn that might be formed on the substrate surface. After deducting the Al_2O_3 component, the EDS spectra in panels f and g indicate that the nanobelt is composed of elements Sn and O.

The crystal structure of the Sn−O nanobelt was determined with transmission electron microscopy (TEM) and selected area electron diffraction (SAED). The TEM image in Figure 2a presents a full ring formed by a closed nanobelt. The single-crystalline nature is confirmed by the sharp SAED patterns along the constituent
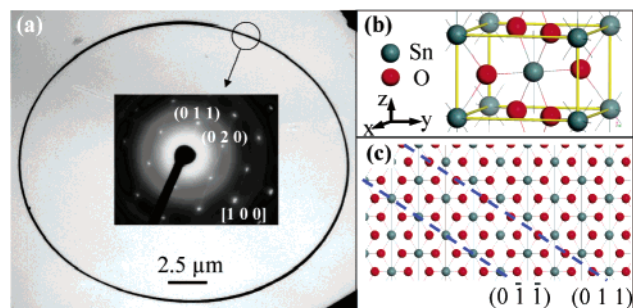
Figure 2. (a) Low magnification TEM image of a SnO$_2$ ring and the corresponding SAED pattern (inset) from the circled region. (b) Tetragonal structure model of SnO$_2$. (c) The structure model of SnO$_2$ projected along [100], displaying the ±(011) polar surfaces.

nanobelt. The SAED pattern in the inset of Figure 2b was taken along the direction normal to the plane of the ring. Analysis of the SAED pattern reveals that the nanobelt has a tetragonal crystal structure with lattice parameters $a = b = 4.75$ Å and $c = 3.20$ Å, which are consistent with the lattice parameters of the rutile SnO$_2$ ($P4_2/mnm$, $a = b = 4.7382$ Å and $c = 3.1871$ Å, JPCDS No. 41-1445). It is noteworthy that the SnO$_2$ belt grows along $\sim$[0$\bar{1}$1] with the side surfaces facing the center of the ring being ±(011) and the top and bottom surfaces parallel to the ring plane being ±-(100). SAED and TEM examination of several other SnO$_2$ nanostructures consistently shows that the nanobelt is dominated by the ±(011) surfaces.

The growth of the ring, spring, and spirals can be understood on the basis of polar surfaces of the rutile-structured SnO$_2$, the atomic model of which is shown in Figure 2b. By projecting the structure model along [100], as shown in Figure 2c, the ±(011) plane can be terminated either solely with Sn^{4+} or solely with O^{2-}, respectively, resulting in a pair of positively and negatively charged polar surfaces on the inner and outer surfaces (or vice versa) of the nanobelt. During the growth at $\sim$500−600 °C in an argon atmosphere, the probability for foreign molecules being adsorbed on the surfaces was negligible within the time of the growth; thus, the polar charges are likely to be preserved. If the charges on the ±(011) side surfaces are not compensated during the growth, the net dipole moment across the side surfaces and the surface energy tend to diverge with an increase of the nanobelt length. On the other hand, the electrostatic energy due to the dipole moment can be minimized or neutralized when the nanobelt rolls up to form a ring or spiral structure. On the other hand, bending of the nanobelt introduces elastic deformation energy, which increases with the decrease of the ring/spiral radius. The minimization of the total energy contributed by electrostatic polarization energy and elastic deformation energy determines the final morphology of the SnO$_2$ nanobelt, resulting in the formation of the ring (Figure 2a) or multiply looped spiral (Figure 1b). Alternatively, if the bending of the nanobelt proceeds during the growth along the axial direction of the curled nanobelt, a helical structure will form (Figure 1a). The spring is formed due to the stretching of the spiral (or multi-looped ring) and/or possibly the electrostatic repulsion between the two adjacent rings.

The above proposed mechanism is consistent with the model established for ZnO.[5] In comparison, the ZnO nanorings/nanosprings reported previously have radii of $\sim$500−800 nm, a nanobelt width of 10−60 nm, and a thickness of 5−20 nm.[5] The radii of the SnO$_2$ rings and springs reported in this paper are 5−50 μm, and the SnO$_2$ nanobelts have widths of a few hundred nanometers and thickness of a few tens of nanometers, which are also larger than those of the ZnO nanobelts. This may be closely related to the charge density on the polar surfaces. The elastic energy increases rapidly with the curvature, width, and thickness of the nanobelt. Accordingly, it is rational to expect much larger helical nanostructures of SnO$_2$ than that of ZnO. In addition, the surface energies of Sn- and O-terminated surfaces can also contribute to the formation of rings and springs. A deep insight on the effect of polarization, elasticity, and surface energy on the nanostructures requires further investigation with first principle computation and more experiments.

In summary, single-crystalline springs, rings, and spirals have been discovered for the first time in a rutile-structured SnO$_2$. The formation of these nanostructures is mainly due to polar surfaces of tetragonal SnO$_2$. The synthesized SnO$_2$ nanostructures are very important for studying the effect of polar surfaces on the morphology of the nanostructures. The research demonstrates that hierarchical nanostructures, which have been observed previously only for polar surface dominated wurtzite ZnO, are also possible in other materials with different crystal structures. Those hierarchical nanostructures may useful for nanoconductors, transparent electrodes, and gas sensors.

Supporting Information Available: More SEM and TEM characterizations of the SnO$_2$ nanobelt. This material is available free of charge via the Internet at http://pubs.acs.org.

References

(1) Pan, Z. W.; Dai, Z. R.; Wang, Z. L. *Science* **2001**, *291*, 1947−1950.
(2) (a) Wang, Y.; Zhang, L.; Meng, G.; Liang, C.; Wang, G.; Sun, S. *Chem. Commun.* **2001**, *24*, 2632−2633. (b) Shi, W.; Peng, H.; Wang, N.; Li, C. P.; Xu, L.; Lee, C. S.; Kalish, R.; Lee, S. T. *J. Am. Chem. Soc.* **2001**, *123*, 11095−11096. (c) Kang, Z.; Wang, E.; Mao, B.; Su, Z.; Gao, L.; Lian, S.; Xu, L. *J. Am. Chem. Soc.* **2005**, *127*, 6534−6535.
(3) (a) Ma, C.; Moore, D.; Li, J.; Wang, Z. L. *Adv. Mater.* **2003**, *15*, 228−231. (b) Jiang, Y.; Meng, X. M.; Liu, J.; Xie, Z. Y.; Lee, C. S.; Lee, S. T. *Adv. Mater.* **2003**, *15*, 323−327. (c) Ma, C.; Ding, Y.; Moore, D.; Wang, X.; Wang, Z. L. *J. Am. Chem. Soc.* **2004**, *126*, 708−709. (d) Jiang, Y.; Meng, X. M.; Yiu, W. C.; Liu, J.; Ding, J. X.; Lee, C. S.; Lee, S. T. *J. Phys. Chem. B* **2004**, *108*, 2784−2787. (e) Johnson, J. C.; Knutsen, K. P.; Yan, H.; Law, M.; Zhang, Y.; Yang, P.; Saykally, R. J. *Nano Lett.* **2004**, *4*, 197−204.
(4) (a) Gao, Y. H.; Bando, Y.; Sato, T. *Appl. Phys. Lett.* **2001**, *79*, 4565−4567. (b) Liu, Z.; Peng, S.; Xie, Q.; Hu, Z.; Yang, Y.; Zhang, S.; Qian, Y. *Adv. Mater.* **2003**, *15*, 936−940. (c) Xi, G.; Peng, Y.; Wan, S.; Li, T.; Yu, W.; Qian, Y. *J. Phys. Chem. B* **2004**, *108*, 20102−20104. (d) Tsai, J. S.; Chen, F. R.; Kai, J. J.; Chen, C. C.; Huang, R. T.; Wang, M. S.; Huang, G. C.; Guo, G. G.; Yu, M. U. *J. Appl. Phys.* **2004**, *95*, 2015−2019. (e) Sigman, M. B.; Korgel, B. A. *J. Am. Chem. Soc.* **2005**, *127*, 10089−10095.
(5) (a) Kong, X. Y.; Wang, Z. L. *Nano Lett.* **2003**, *3*, 1625−1631. (b) Kong, X. Y.; Wang, Z. L. *Appl. Phys. Lett.* **2004**, *84*, 975−977. (c) Kong, X. Y.; Ding, Y.; Yang, R.; Wang, Z. L. *Science* **2004**, *303*, 1348−1351. (d) Yang, R.; Ding, Y.; Wang, Z. L. *Nano Lett.* **2004**, *4*, 1309−1312.
(6) Gao, P. X.; Ding, Y.; Mai, W.; Hughes, W. L.; Lao, C. S.; Wang, Z. L. *Science* **2005**, *309*, 1700−1704.
(7) Duan, J. H.; Yang, S. G.; Liu, H. W.; Gong, J. F.; Huang, H. B.; Zhao, X. N.; Tang, J. L.; Zhang, R.; Du, Y. W. *J. Cryst. Growth* **2005**, *283*, 291−296.
(8) Maiti, A.; Rodriguez, J. A.; Law, M.; Kung, P.; McKinney, J. R.; Yang, P. *Nano Lett.* **2003**, *3*, 1025−1028.
(9) Dai, Z. R.; Pan, Z. W.; Wang, Z. L. *J. Am. Chem. Soc.* **2002**, *124*, 8673−8680.

JA0578000